PLANETARY SCIENCE

Paleoseismic activity in the moon's Taurus-Littrow valley inferred from boulder falls and landslides

Thomas R. Watters[1]* and Nicholas C. Schmerr[2]

The Taurus-Littrow valley offers a unique opportunity to analyze surface changes due to seismic activity on the lunar surface. Ground acceleration from moonquakes has triggered landslides and boulder falls in the valley. The formation and growth of the Lee-Lincoln thrust fault is a likely source of the moonquakes. Here, we estimate the ground acceleration and quake magnitude for four boulders and one landslide: all sampled by Apollo 17 astronauts. These features all have exposure ages that establish the approximate timing of the moonquakes. Our analysis suggests that the structural relief of the Lee-Lincoln fault scarp is the result of multiple coseismic slip events with a minimum body wave magnitude M_w of ~2.9 to 3.3. The formation and growth of thousands of such globally distributed young thrust faults, through multiple coseismic events, suggest that the Moon has a history of widespread strong shallow moonquakes. Shallow moonquakes from likely active faults may pose a potential hazard to long-term outposts.

INTRODUCTION

Seismic activity on the Moon has numerous sources, both exogenic and endogenic in origin. The effects of ground acceleration from moonquakes, particularly shallow moonquakes that are the most energetic of the events recorded by the Apollo Passive Seismic Network (*1*), manifest in many forms of surface change. The most obvious are landslides (*2*, *3*) and boulder falls (*4*–*9*). A prominent feature in the Taurus-Littrow valley emplaced by a landslide emanating from South Massif is the light mantle deposit, consisting of high albedo material that is draped over the valley floor and the Lee-Lincoln fault scarp (*10*–*13*). Evidence of a lower reflectance unit within the light mantle deposits suggests two landslide events (*10*). Alternatively, it has been suggested that the light mantle deposit is a ray formed from Tycho ejecta (*14*). Exposure ages of the regolith fragments collected at Station 2 and 3 indicate an age of the light mantle deposits of 70 to 110 million years (Ma), consistent with the estimated age of the Lee-Lincoln fault (*11*).

The Apollo 17 landing site in the Taurus-Littrow valley has numerous boulders that rolled down slopes of North and South Massifs (*10*, *11*, *15*, *16*). Boulder falls in the valley may be from impact ejecta; however, boulder falls located at the base of North and South Masiffs can be traced by trails back to their sources where no fresh impact craters are found. Boulder falls from impact ejecta can be distinguished from those induced by seismic shaking. Impact-ejected boulders typically have radially arranged trails, shorter trail lengths, and trails in the regolith that are narrower and shallower (*8*, *9*). Of the boulders examined by Apollo 17 astronauts Cernan and Schmitt at Stations 2, 6, and 7, the Station 6 boulder is the largest, measuring roughly 15 m by 8 m (*16*). The more typical scale of boulders at the base of the North and South Massif is a few meters or less in size. The fall of the Station 6 boulder down the slopes of North Massif left a clear narrow ditch or boulder track in the regolith (Figs. 1 to 3) (*15*, *17*).

Samples of boulders, specifically, the Station 2 boulders 1 and 2, the Station 6 boulder, and the Station 7 boulder, allow the determination of cosmic ray exposure ages that indicate how long the boulders have been at their present locations (*18*, *19*). This provides a more direct way of dating events over relative approaches like crater counting (*5*). The exposure ages of these boulders and the light mantle deposit establish the approximate timing of the mass wasting events in the Taurus-Littrow valley. Here, we postulate and test the hypothesis that these events were triggered by seismic shaking.

RESULTS

We estimate the amount of ground acceleration needed to trigger a regolith landslide using a relationship involving the factor of safety (F_S) (see Materials and Methods). The landslide that emplaced the light mantle deposit that covers part of the Taurus-Littrow valley floor is likely from a shallow moonquake due to the formation of or a slip event on the Lee-Lincoln fault (*11*). For a 1-m-thick landslide of regolith with low cohesion (0.1 kPa) on slopes of ~25° near the top of South massif, where the $F_S > 1$ (assuming an angle of internal friction ϕ of 30°), a lower limit ground accelerations of ~0.223 ms^{-2} or ~14% g_{lunar} is needed (Table 1). Assuming a substantially greater regolith cohesion (0.5 kPa), an upper limit of the ground acceleration needed to trigger the South Massif landslide is estimated to be ~0.464 ms^{-2} or ~29% g_{lunar}. A younger, second landslide is suggested by a lower reflectance unit within the light mantle deposit (*11*).

We also introduce a simple relation to estimate the ground acceleration needed to dislodge boulders that have fallen from the slopes of North and South Massifs (see Materials and Methods). Applying this relation to boulders 1 and 2 at Stations 2 and Station 6 and 7 boulders (Fig. 3), it is estimated that minimum ground accelerations of ~0.42 to ~0.55 ms^{-2} or ~26 to ~34% g_{lunar} are needed to trigger the boulder falls (Table 1). It is assumed that the dimensions of the post-fall boulders are not considerably different from their pre-fall dimensions. These values should be considered the minimum ground acceleration needed to trigger a fall, because they assume an optimum initial position of the boulder, that is, the boulder rests on its short axis (w) with its long axis (h) vertical ($h/w > 1$). It also assumes that the boulders are free to roll, i.e., not restrained by partial burial in regolith or frictional attachment to a bedrock outcrop. If the boulders are resting on their long axis with the short axis vertical $h/w < 1$, then appreciably greater ground acceleration is required (Fig. 4A). This may account for the stability or resistance to

[1]Smithsonian Institution, Washington, DC, USA. [2]University of Maryland, College Park, MD, USA.
*Corresponding author. Email: watterst@si.edu

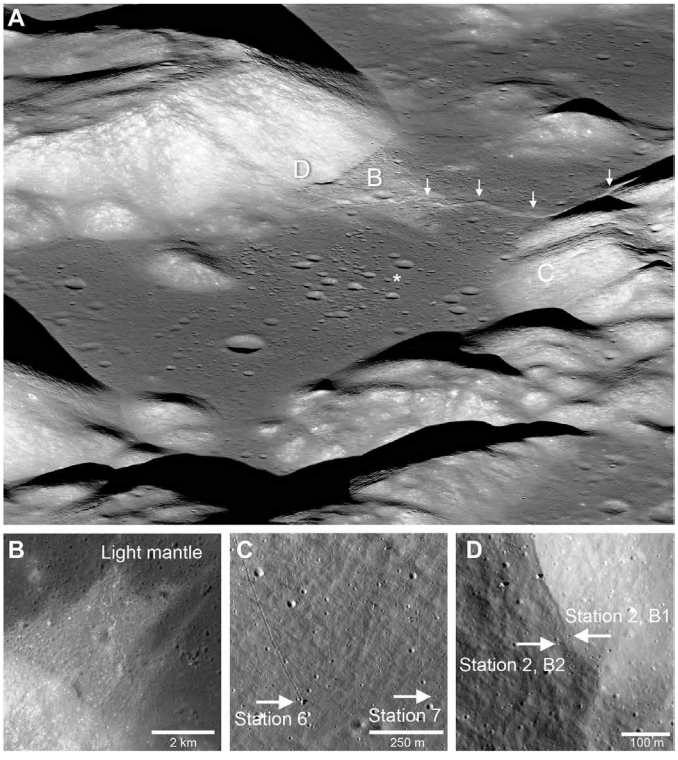

Fig. 1. The Taurus-Littrow valley and the Lee-Lincoln fault scarp. (**A**) Lunar Reconnaissance Orbiter Camera Narrow Angle Camera (LROC NAC) oblique of the valley. The Lee-Lincoln fault scarp cuts across the valley floor (arrows). (**B**) The light mantle landslide deposit across the valley floor from South Massif. (**C**) Apollo 17 mission Station 6 and 7 boulders at the base of North Massif (arrows). (**D**) Apollo 17 Station 2, boulders 1 and 2 at the base of South Massif. The approximate locations of the boulders and light mantle landslide deposit are shown in (A) by panel letters. The asterisk shows the approximate location of the Apollo 17 Lunar Module.

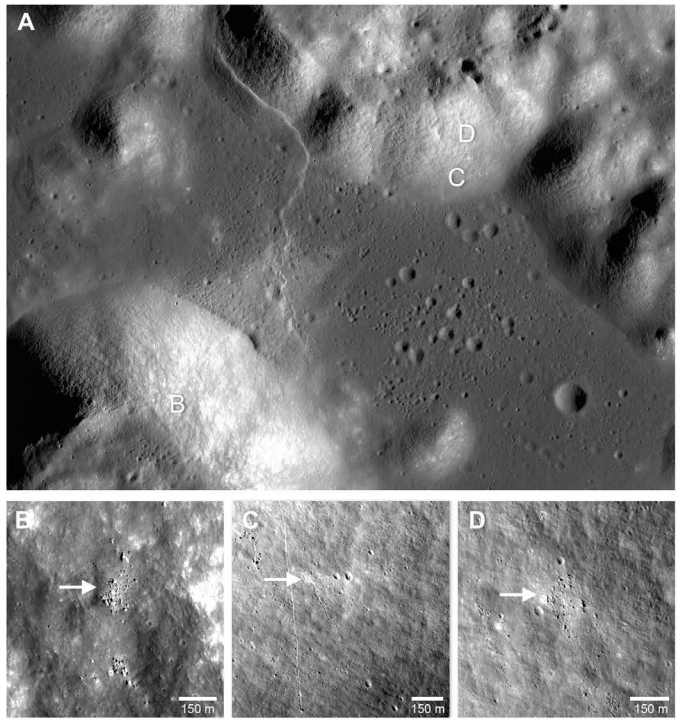

Fig. 2. Taurus-Littrow valley and boulder source areas. (**A**) LROC NAC mosaic nadir view of the valley and North and South Massifs. (**B**) Boulder field source area of Station 2, boulders 1 and 2 (arrow). (**C**) Boulder field source area of Station 6 boulder (arrow). (**D**) Boulder field source area of the Station 7 boulder (arrow). The approximate locations of the boulder source areas are shown in (A) by the panel letters.

rolling of other boulders in the source regions (Fig. 2). The upper limit of the ground acceleration can be obtained by assuming that the initial position of the boulders is resting on their long axis (long axis horizontal) and that the short axis is vertical $h/w < 1$. Assuming this configuration, we find that the maximum ground accelerations ranges of ~1.24 to ~1.814 ms^{-2} or ~77 to ~112% g_{lunar} (Table 1).

To evaluate the magnitude and effect of seismic shaking in the Taurus-Littrow valley and determine whether the predicted peak ground acceleration to trigger the boulder falls and landslide are reasonable for a realistic magnitude shallow moonquake, we generated regional shake models for a notional slip event on the Lee-Lincoln fault. The simulation is for the moment magnitude (M_w) = 3.0 event located at the Lee-Lincoln, at a source depth of 100 m (Fig. 5). Plots of the model decay in vertical and horizontal shaking with distance from the epicenter show that the minimum predicted ground shaking needed to trigger the landslide and boulder falls in the source areas is consistent with the ground motion predicted in an $M_w = 3.0$ quake (Fig. 5, A and C).

The elastic wave propagation at the fault is modeled using the Serpentine Wave Propagation Program (WPP) computer code (*20*). WPP uses an anelastic, finite-difference, second-order accuracy scheme that includes mesh refinement and a grid that allows for a topography-defined free surface. The code incorporates stochastic heterogeneous materials that produce lunar-like crustal conditions where there is strong scattering and heterogeneity in the megaregolith. In Fig. 6, we compare our simulation results to the Apollo 16 SIVB impact to illustrate the similarity of the calculated waveforms to a near-surface shallow moonquake event, noting that the impact source may vary from a shallow tectonic event and that no shallow events were ever recorded this close to the source. The surface and body waves in the WPP simulation become strongly depolarized at ~25 km from the source and are diffusive in character, at distances that are shorter than those modeled for the artificial impacts shown in ground-motion modeling (*21*).

The simulations are designed to capture the waveform effects for the Taurus-Littrow valley. Our background model for the shakemap simulations uses the Lunar Orbiter Laser Altimeter topographic model for surface elevation of the region (*22*) and assumes the seismic velocity structure described in (*23*). A von Karman random distribution (*23*) of velocities and densities with 25% peak-to-peak variation with a 100-m autocorrelation length is imposed on the uppermost 1 km of regolith to produce scattering effects and diffuse ground motion. We impose a scattering structure that is more diffusive than the 5 to 10% heterogeneity and autocorrelation length of 650 m in the study by Onodera *et al.* (*21*) to capture near source regolith and megaregolith heterogeneity. The simulation grid is a 100 km–by–100 km–by–60 km deep box, with grid spacing h set to 60 m. Grid refinements are implemented at depths of 38 km ($h = 30$ m), 15 km ($h = 15$ m), and 1 km ($h = 7$ m) to maintain wavefield stability at the simulation frequency < 1.25 Hz and to maintain computational efficiency. The source is centered in the box and imposed as a double

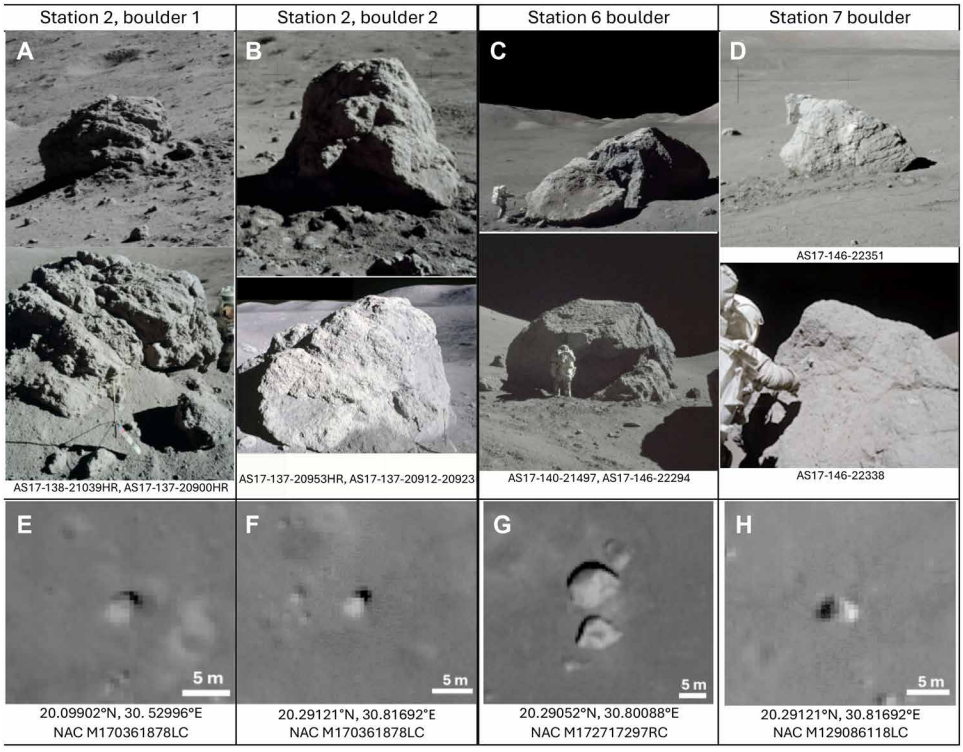

Fig. 3. Boulders examined and sampled by the Apollo 17 astronauts Eugene Cernan and Harrison Schmitt. (**A**) Apollo 17 boulder 1 at Station 2. (**B**) Apollo 17 boulder 2 at Station 2. (**C**) Station 6 boulder. (**D**) Station 7 boulder. (**E** to **H**) LROC NAC nadir images of the boulders.

Table 1. Landslide and boulder falls in Taurus-Littrow valley. Exposure ages and boulder dimensions are from Arvidson *et al.* (*18, 19*), and Schmitt *et al.* (*11*).

Feature type	Location source	Boulder dimension (m)	Exposure ages/ average ages (Ma)	Ground acceleration min/max (ms^{-2})	Source slope (°)	Source distance (m)
Light mantle	South Massif 20.1666°N, 30.5399°E	$t = 1$	~70–110 (90)	0.223/0.464	~25.0	4898.73
Station 2, boulder 1	South Massif 20.0985°N, 30.5293°E	$h = 1$ $w = 2$	~45–55 (40)	0.416/1.662	~29.4	4423.73
Station 7 boulder	North Massif 20.2883° N, 30.8149° E	$h = 3$ $w = 1.5$	~25–32 (28.5)	0.425/1.701	~28.8	7050.37
Station 2, boulder 2	South Massif 20.0985°N, 30.5293°E	$h = 3$ $w = 2$	~22	0.554/1.247	~29.4	4423.73
Station 6 boulder	North Massif 20.2904° N, 30.8011° E	$h = 15$ $w = 8$	~17–21 Ma (19)	0.516/1.814	~25.8	6682.03

couple (strike = 0°, dip = 35°, and rake = 90°) 100 m below the surface elevation. The simulation is run to 250 s, approximately when surface waves start to interact with the absorbing boundary sides of the box (Fig. 6A). We capture full ground-motion time series at stations positioned every kilometer in the x and y directions of the box (see example in Fig. 6B) and compute waveform envelope of the waveforms to determine peak ground shaking for our following boulder fall analysis.

The modeled wavefield shows that the region of modified Mercalli scale values of "weak" (<0.029 m/s^2) to "light" (<0.26 m/s^2) seismic shaking extends well into the Taurus-Littrow valley and up both North and South Massifs (Fig. 5, C and D). A comparison of the boulder fall source locations with the model shake model shows that all the boulder source areas are within the "light" (<0.26 m/s^2) to "moderate" (<1.13 m/s^2) shaking range (Fig. 5, A and B) if the boulder initial position is optimum ($h/w > 1$) and are within "moderate"

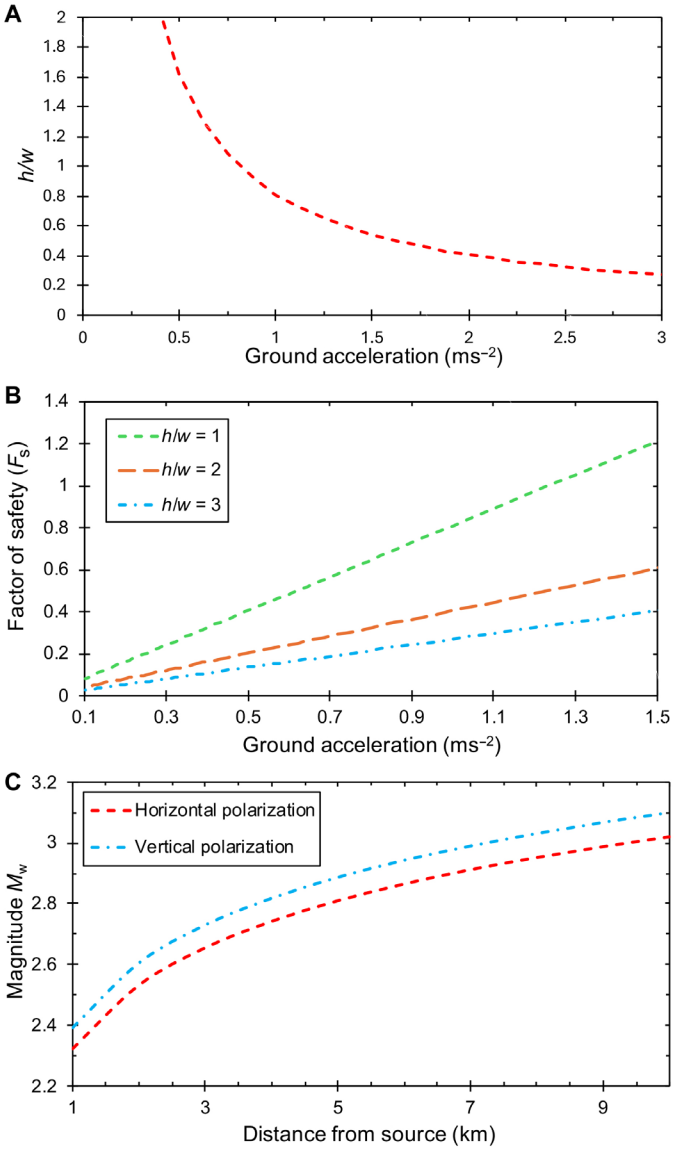

Fig. 4. Effect of boulder aspect ratio and F_S on critical ground acceleration to trigger a fall. (**A**) As the *h/w* ratio of a boulder increases, the ground acceleration needed to induce a boulder to roll decreases, for a boulder resting on a surface slope of a given F_S. (**B**) The ground acceleration needed to induce a boulder roll is greater if the boulder rests on a surface slope with an $F_S > 1$ even for boulders with an $h/w > 1$. (**C**) Magnitude as a function of distance from the quake source for a given ground acceleration using values for parameters *b*, *c*, and *d* from the elastic wave propagation models for vertical and horizontal polarization (Table 2).

(<1.13 m/s^2) to "strong" (<2.10 m/s^2; exceeding lunar *g*) if the boulder initial position is not optimum ($h/w < 1$). Thus, the simulation suggests that the predicted ground acceleration for an $M_w = 3.0$ quake was sufficient to dislodge the four boulders examined in the study and trigger the light mantle landslide. We note that an $M_w = 3.0$ equivalent bolide impact (10 to 100 kilotons of TNT) with similar amounts of energy would require formation of a nearby impact crater with a diameter between 50 and 400 m, depending upon impact angle, target material, and bolide velocity (*23*). No fresh primary impact crater of this diameter range is present at <30 km of the Taurus-Littrow valley; however, a cluster of secondaries attributed to Tycho ejecta are present and likely contributed seismic shaking in the valley (*24*).

From estimates of the seismic shaking, the magnitude of the associated quakes can be constrained (see Materials and Methods). The exposure ages of the fallen boulders and the light mantle landslide and the estimates of the M_w of the quakes allow a history of some of the paleoseismic activity related to the formation and growth of the Lee-Lincoln fault to be proposed (Fig. 7). The minimum and maximum M_w estimated to have caused the boulder falls and the landslide are ~2.9 to 3.1 and ~3.1 to 3.4 (Fig. 7A), respectively, using values for *b*, *c*, and *d* from the vertical polarization ground-motion models and ~2.8 to 3.0 and ~3.0 to 3.3 (Fig. 7B) using values for horizontal polarization ground-motion models (see Eq. 6 and Materials and Methods) (Table 2). These ranges are below the median M_w of 4.5 estimated for the shallow moonquakes recorded by the Apollo Passive Seismic Network (*25*).

The oldest event of those dated by exposure age is the landslide that emplaced the light mantle deposit ~90 Ma. The lower reflectance unit of the light mantle deposit was not sampled, although Schmitt *et al.* (*11*) suggest that it may be older due to longer exposure to space weathering. We hypothesize that the light mantle deposit landslide event was associated with the initial shallow moonquake and resulting ruptures that formed the Lee-Lincoln thrust fault with an estimated M_w of ~2.85 to ~3.01 (Fig. 7) (Table 1). The next four seismic events with $M_w \geq$ ~3.0 are assumed to be subsequent slip events on segments of the Lee-Lincoln fault over an ~70-Ma period (Fig. 7). If correct, this suggests that the structural relief and total displacement on the fault accumulated over a minimum of five coseismic events. The analysis suggests that the strongest moonquake in the Taurus-Littrow valley in the past ~90 Ma was a minimum of ~3.1 (Fig. 7). This analysis also suggests that the boulder falls are an expression of the strongest seismic events in the Taurus-Littrow valley over the past ~90 Ma and that the regolith landslides required less ground motion to be triggered than did the boulder falls. It may be the case, in general, for the Moon, that landslides on unstable slopes will be the expected surface expression of weak or light seismic shaking.

Another indication of seismic shaking effects throughout the entire Taurus-Littrow valley is seen in the degradation rate of small craters in basalt regolith of the valley (*26*). It is higher than in the Apollo 16 Cayley plains (~9°S, 15.5°E), and the depth-diameter ratio of the degraded craters does not change as a function of distance from the Lee-Lincoln scarp (a distance of >15 km) (*26*). This suggests the possibility of a recent history of repeated strong seismic shaking from slip events on the Lee-Lincoln thrust fault.

DISCUSSION

The implication for the globally distributed population of young thrust faults that number in the thousands (*2*, *27*, *28*) is that they likely developed and grew as a result of multiple coseismic slip events that have resulted in recent boulder falls and landslides all over the Moon rather than in single larger rupture events. The results of this study also suggest that the young thrust faults could continue to pose a potential hazard to future lunar outposts and long-term habitations and supporting infrastructure on the Moon. If a shallow moonquake with its source on the Lee-Lincoln fault had occurred at a magnitude of those estimated by the landslide and boulder falls analyzed here ($M_w = 2.9$ to 3.4), then the modeling suggests that seismic shaking

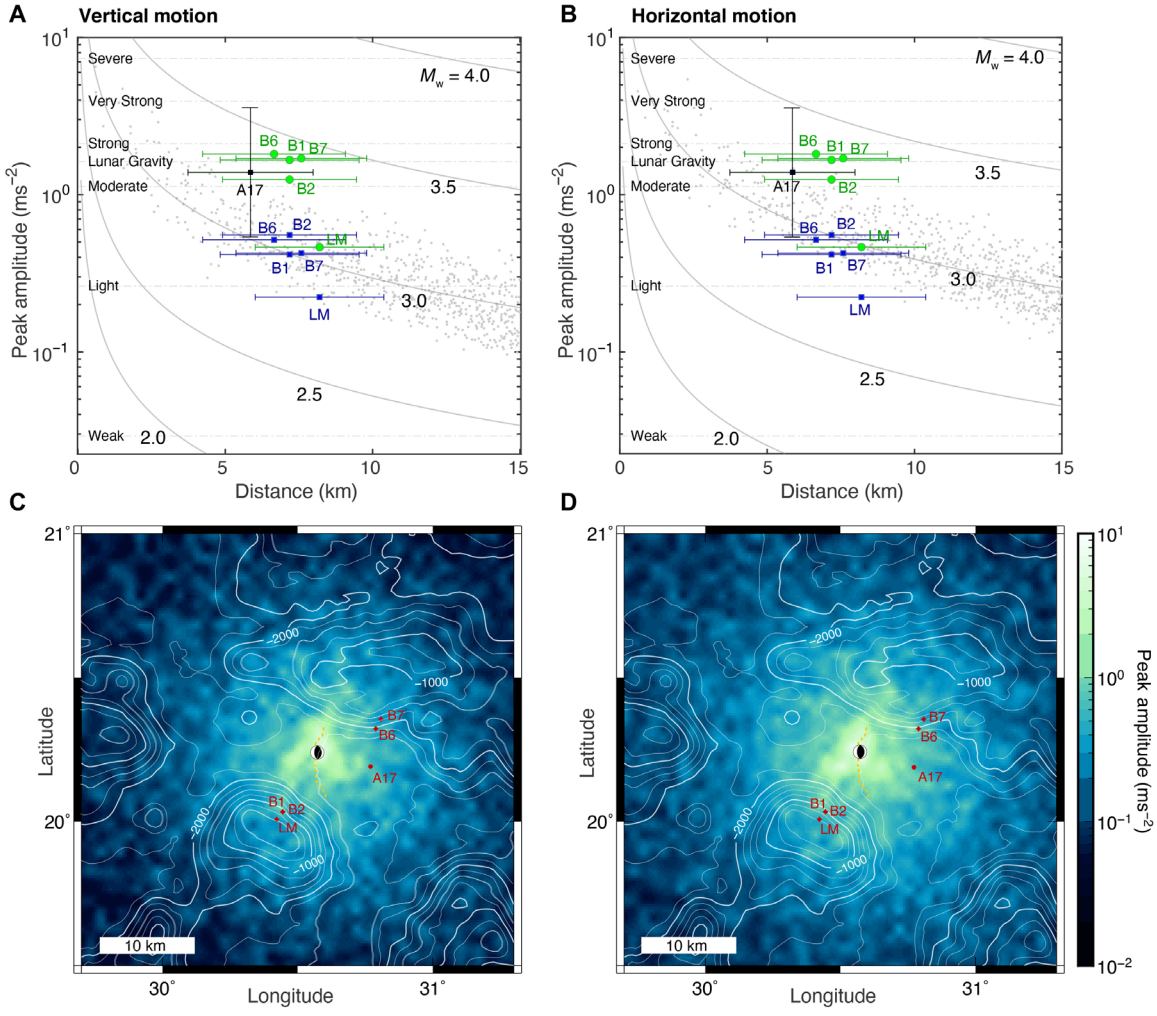

Fig. 5. Seismic shakemaps and expected ground motion for a slip event on the Lee-Lincoln thrust fault. The moonquake is situated at 20.23848°N, 30.57286°E for a dip slip event with a 3.0 M_w hypocenter at 100-m depth (blue outline). The top plots show (**A**) the decay in vertical shaking and (**B**) and horizontal shaking with distance from the epicenter. Gray circles show the peak ground shaking across the three-dimensional model domain at distance from the source. The uncertainty in M_w is drawn from these values is identical across the boulder sites and indicated on the A17 site. The isoseismals are plotted for M_w of 2.0 to 4.0 with the model peak ground acceleration shown relative to the modified Mercalli intensity scales. The predicted ground acceleration needed to trigger the boulder falls and landslide is plotted (LM, light mantle landslide; B1, Station 2, boulder 1; B2, Station 2, boulder 2; B6, Station 6 boulder; B7, Station 7 boulder) for the minimum estimate (blue) and maximum estimate (green). The predicted ground acceleration at the Apollo 17 landing site is also shown. The error bars show the range in predicted ground shaking for the boulders and landslide with optimum and less than optimum initial conditions and the uncertainty in the epicenter location along the Lee-Lincoln fault. The bottom two shakemaps show (**C**) the peak vertical acceleration and (**D**) horizontal acceleration. The source locations of the boulders and LM landslide are shown on the maps. The location of the Apollo 17 landing site is show on the maps (A17).

could have been between 0.2 and 2.1 m/s^2 at the Apollo 17 Lunar Module (LM) location of ~5.9 km to the east of the fault. If this had occurred during the landed phase of the Apollo 17 mission, then, from Eq. 5, we estimate that the peak acceleration needed to compromise the stability of the 9.4-m-wide and 5.5-m-tall Lunar Module was 1.38 m/s^2 for a $F_S = 1$; any ground motion greater than this would have put the safety of the Lunar Module and astronauts at risk.

The probability of a hazard-level moonquake can be assessed with an estimate of the recurrence interval on the Lee-Lincoln fault. The frequency-magnitude relation of the quakes is expressed by the Gutenberg-Richter relation ($\log_{10} N = a - bM$), where N is the number of quakes with magnitudes of $\geq M$ over an interval of time, and a and b are constants (*29*). Assuming a b value (the slope of the frequency-magnitude plot of recorded shallow moonquakes) of 1 and $M = 3.25$ (the average magnitude of the evaluated events), a that depends on the number of quakes on the fault over the period is here estimated as 3.9490 on the basis of our five events. Thus, over the 50-Ma period, ~8.9 moonquakes of magnitude $M_w = 3.0$ would be expected, as well as 0.89 quakes of $M_w = 4.0$ and 0.089 quakes of $M_w = 5.0$. If the threshold for hazard is assumed to be light to moderate shaking, then this level of shaking will only be exceeded at distances of 1 to 2 km from the fault for $M_w = 2.0$ events and at 5 to 15 km for $M_w = 3.0$ quakes. The recurrence interval for the Lee-Lincoln fault $R_i \sim t/N$ where $N = 8.9$ and $t = 50$ Ma (period between assumed fault formation age and age of the next major seismic event, Table 1) is estimated to be ~5.6×10^6 years. Thus, the chance of a potentially

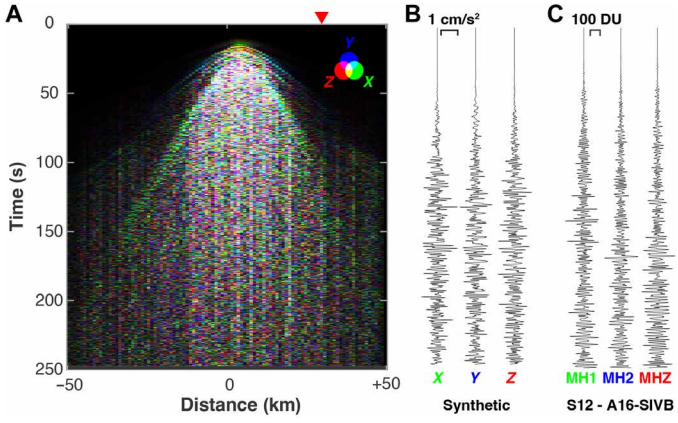

Fig. 6. Comparison of the predicted ground-motion waveforms for the Lee-Lincoln scarp to seismic recordings from Apollo. (**A**) polarization of the wavefield from the M_w = 3.0 simulation for a 1-km spacing station array located North-South of the source. Waveform amplitudes are scaled to unity, and polarization is assigned to the red (*Z*), green (*X*), and blue (*Y*) polarization directions. Uniform partitioning of each component onto the color space will produce white, while polarized energy will show as the respective colors. The strongly polarized arrivals close to the source decay to unpolarized energy at >25 km from the source. (**B**) Waveforms for a station placed at 30 km from the source showing the amplitudes of the ground motion in digital units (DU) and scattering characteristics of the simulated wavefield. (**C**) Waveforms from the Apollo 12 seismic station for the impact of the Apollo 16 SIVB capsule on 19 April 1972 at 20:53:01, the data are low-pass filtered to 2 Hz. MH1, MH2, and MHZ are the *X*, *Y*, and *Z* mid-period Apollo seismometer sensors.

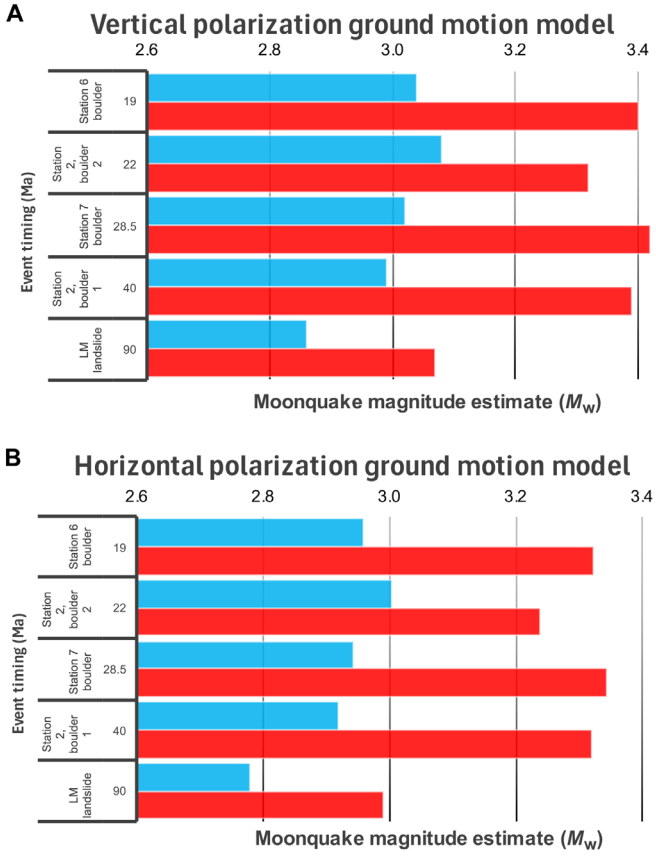

Fig. 7. Paleoseismic events in the Taurus-Littrow valley. (**A**) Estimates of mean M_w using Eq. 3 and values of constants derived for vertically polarized ground motion (Table 2). (**B**) Estimates of M_w using values of constants derived for horizontally polarized ground motion (Table 2). Blue bars are minimum mean estimated M_w for boulders in optimum pre-fall configurations and LM landslide with minimum regolith cohesion (see text for details). Red bars are maximum mean M_w for boulders and landslide assuming high regolith cohesion. The timing of events is average exposure ages determined from samples collected by the Apollo 17 astronauts (Table 1).

hazardous event once every t/$N(M_w\ 3.0)$ years at a distance <15 km from the Lee-Lincoln fault is ~1 of 56,000 or ~0.000018% in a given year or ~1 of 5600 or ~0.00018% per decade. The chance of a potentially hazardous quake in the Taurus-Littrow valley on any given day is then ~1 of 20,000,000 or ~5×10^{-8}%. Thus, the probability that a hazardous moonquake could have occurred during the Apollo 17 mission was extremely low. This should be considered a lower limit, because the Lee-Lincoln fault over this period was likely the source of more than the five events evaluated here. In that case, the value of *a* would increase along with the probability of a hazardous quake, i.e., if there were 10 times more events that produced no boulder falls, then the risk would be 10 times higher.

Future missions with higher aspect ratio landers, such as the Starship Human Landing System, with an estimated height of 50 m and width of 9 m, would require a factor of 10 less ground motion than boulders to create adverse shaking effects (e.g., an $M_w = 2.6$ at the same distance to Lee-Lincoln fault would potentially be problematic for a taller spacecraft). Although the likelihood of a shallow moonquake occurring during a short-duration crewed mission is extremely low, future missions can mitigate the risk primarily by keeping their distance from recent surface-breaking faults as recurrence likelihood is low and shaking rapidly drops off with distance. Particular attention should be given to avoid locating landed assets and long-lived infrastructure in areas where slopes are determined to be unstable and where boulder fields are perched on elevated slopes.

The results further suggest that recent boulder falls and landslides elsewhere on the Moon (and other airless bodies) can be used to approximate the strength of quakes that triggered them. Given the dimensions of a boulder that has fallen and the location of the source area, the ground acceleration and minimum and maximum magnitude of the quake can be estimated.

MATERIALS AND METHODS

Critical ground acceleration—landslide

The ground acceleration necessary to trigger a regolith landslide of a given thickness can be estimated using a relationship involving the F_S, which describes the ratio of shear strength to shear stress for downslope movement (*30*). While other sophisticated analysis tools have been used to predict the effects of earthquakes on the stability of granular slopes and landslide occurrence [e.g., (*31*, *32*)], here, we use the sliding block model of Newmark (*33*).

The critical ground acceleration a_C necessary to trigger a regolith landslide of thickness *t* as a function of surface slope is given by

$$a_C(\theta) = \left(F_S - 1\right) g \ \sin\theta \qquad (1)$$

where the slope stability is characterized by F_S. For a dry, cohesionless material, F_S is given by

Table 2. WPP model–derived constants. See the main text for explanation.

Constant	Vertical polarization	Horizontal polarization
b	0.00010746 ± (0.0001062, 0.0001087)	0.00013656 ± (0.0001351, 0.000138)
c	1.50	1.50
d	1.0621 ± (1.068, 1.056)	1.0456785 ± (1.051, 1.040)

$$F_S = \frac{\tan\phi}{\tan\theta} \quad (2)$$

where ϕ is the angle of internal friction and θ is the surface slope. Unstable slope conditions are when $F_S < 1$, and stable slope conditions are when $F_S > 1$. For a dry material with finite cohesion like the lunar regolith, F_S as a function of θ is given by

$$F_S(\theta) = \left(\frac{C}{\rho_r g t \sin\theta} + \frac{\tan\phi}{\tan\theta}\right) \quad (3)$$

where the shear stress is $\rho_r g t \sin\theta$, ρ_r is the material density, g is the acceleration due to gravity, t is the landslide thickness, and the shear strength is the cohesion of the material C (*33*, *34*). The key parameters to slope stability of the lunar regolith are the surface slope, the angle of internal friction, the regolith cohesion, and the regolith bulk density. Of the key parameters, the cohesion has the greatest influence on F_S (*30*). Analysis of the critical ground acceleration a_C as a function of θ shows that, for a realistic range of C (0.1 to 1.0 kPa) and a fixed ϕ of 30°, the ground acceleration needed to trigger a regolith landslide decreases linearly with increasing θ, with greater regolith cohesion providing greater slope stability (*30*).

Critical ground acceleration—boulder falls

A simple relation to estimate the ground acceleration needed to dislodge a boulder resting on a sloping surface using an approach involving torque (or the force needed to induce rotation) is proposed. The equilibrium or static condition of a cuboid-shaped boulder of a given height h, width w, and length l, at rest can be expressed as

$$mah = mg\frac{w}{2} \quad (4)$$

where w is assumed to be the maximum dimension of the width or length of the base of the boulder, m is mass, a is acceleration, and g is the acceleration due to gravity. A critical ground acceleration would cause the boulder to topple over and roll. To account for the surface slope and the angle of internal friction of the slope that the boulder is resting on, we scale a by the factor of safety F_s for a cohesionless material (Eq. 2). The simple relation for the critical ground acceleration a_c then becomes

$$a_c = \frac{gw}{2h}\left(\frac{\tan\phi}{\tan\theta}\right) \quad (5)$$

It should be noted that, in this derivation, the mass terms m drop out. This relation suggests, for a given F_s as the h/w ratio increases, the ground acceleration needed to induce a boulder to roll decreases (Fig. 4A). Conversely, as the ratio decreases and the boulder is wider than it is high $h/w < 1$, the ground acceleration needed increases. Also, if the boulder rests on a surface slope with an $F_S > 1$, then the ground acceleration needed to dislodge it is greater even for boulders with an $h/w > 1$ (Fig. 4B). A study of lunar rocks and boulders morphologies indicates a height to maximum-diameter (h/D) ratio of 0.5 (*35*). It has been suggested that impact-ejected lunar rocks and boulders should lie with their short axes upward, suggesting that most lunar boulders lie on their long axes (*36*).

Quake magnitudes

From the study of earthquakes, it has been shown that ground acceleration a varies with quake magnitude M and distance r from the source and can be approximated by the relation

$$a(M, r) = b10^{cM}r^{-d} \quad (6)$$

where b, c, and d are constants (*29*). The constant b depends on the type of ground motion (velocity, displacement, or acceleration) and is related to the frequency and absolute amplitude, c is the relative amplitude predicted between magnitudes and is derived from the seismic moment equation, and d is related to the distance from the source and is a function of the structure and attenuation in the geologic medium. Solving this equation for M

$$M = \frac{1}{c}\left[\log10\left(\frac{a}{b}\right) + d\log10(r)\right] \quad (7)$$

and using values for b, c, and d obtained from the WPP simulation for vertical and horizontal polarization ground-motion model (Table 2), estimates of M can be made from the predicted seismic shaking needed to trigger the boulder falls and landslide (Table 1). The body wave magnitudes of the moonquakes estimated in the Taurus-Littrow valley, about $M_w = 3$, are in the low range of shallow moonquakes recorded by the Apollo Passive Seismic Network (*25*, *37*). The M_w necessary to trigger a landslide or boulder fall for a given critical ground acceleration increases with increasing distance from the quake source, including surface distance and event depth (Fig. 4C).

REFERENCES AND NOTES

1. Y. Nakamura, G. V. Latham, H. J. Dorman, A. K. Ibrahim, J. Koyama, P. Horvath, "Shallow moonquakes: Depth, distribution and implications as to the present state of the lunar interior," in *Proceedings of the Tenth Lunar and Planetary Science Conference*, R. B. Merrill, Ed. (Pergamon, 1979), pp. 2299–2309.
2. T. R. Watters, R. C. Weber, G. C. Collins, I. J. Howley, N. C. Schmerr, C. L. Johnson, Shallow seismic activity and young thrust faults on the Moon. *Nat. Geosci.* **12**, 411–417 (2019).
3. T. R. Watters, E. J. Speyerer, M. S. Robinson, "Recent landslides and their relations to young thrust fault scarps on the moon," in *53rd Lunar and Planetary Science Conference* (The SAO Astrophysics Data System, 2022), p. 1626.
4. P. Senthil Kumar, U. Sruthi, N. Krishna, K. J. P. Lakshmi, R. Menon, Amitabh, B. G. Krishna, D. A. Kring, J. W. Head, J. N. Goswami, A. S. Kiran Kumar, Recent shallow moonquake and impact-triggered boulder falls on the Moon: New insights from the Schrödinger basin. *J. Geophys. Res. Planets* **121**, 147–179 (2016).
5. P. Senthil Kumar, R. Mohanty, K. Jaya Prasanna Lakshmi, S. T. G. Raghukanth, A. C. Dabhu, R. P. Rajasekhar, R. Menon, The seismically active lobate scarps and coseismic lunar boulder avalanches triggered by 3 January 1975 (M_W 4.1) shallow moonquake. *Res. Lett.* **46**, 7972–7981 (2019).

6. V. T. Bickel, J. Aaron, A. Manconi, S. Loew, U. Mall, Impacts drive lunar rockfalls over billions of years. *Nat. Commun.* **11**, 2862 (2020).
7. T. Ruj, G. Komatsu, K. Kawai, H. Okuda, Z. Xiao, D. Dhingra, Recent boulder falls within the Finsen crater on the lunar far side: An assessment of the possible triggering rationale. *Icarus* **377**, 114904 (2022).
8. R. Mohanty, P. Senthil Kumar, S. T. G. Raghukanth, K. J. P. Lakshmi, The long-lived and recent seismicity at the lunar orientale basin: Evidence from morphology and formation ages of boulder avalanches, tectonics, and seismic ground motion. *J. Geophy. Res. Planets* **125**, e2020JE006553 (2020).
9. R. Mohanty, P. Senthil Kumar, K. J. P. Lakshmi, V. Krishnan, A. Mishra, G. S. S. Karthik, Evidence for trail forming ejecta boulder falls around fresh simple impact craters at the lunar Orientale multi-ring basin and implications for ballistic ejecta sedimentation on the Moon. *Icarus* **405**, 115723 (2023).
10. H. H. Schmitt, Apollo 17 report on the valley of Taurus-Littrow. *Science* **182**, 681–690 (1973).
11. H. H. Schmitt, N. E. Petro, R. A. Wells, M. S. Robinson, B. P. Weiss, C. M. Mercer, Revisiting the field geology of Taurus-Littrow. *Icarus* **298**, 2–33 (2017).
12. G. Magnarini, T. M. Mitchell, P. M. Grindrod, H. H. Schmitt, N. E. Petro, Scaling relationship between the wavelength of longitudinal ridges and the thickness of long runout landslides on the moon. *Moon* **126**, e2021JE006922 (2021).
13. M. Neuman, B. L. Jolliff, K. Wang, N. Petro, J. Valenciano, C. R. Neal, S. Eckley, J. Kent, L. Sun, P. Lucey, S. Bell, K. Helen Joy, R. Tartese, R. Jones, P. Carpenter, R. V. Morris, N. C. Haney, S. Simon, M. Cato, C. K. Shearer, K. C. Welten, K. Nishiizumi, M. W. Caffee, R. A. Colina-Ruiz, T. Kroll, D. Sokaras, H. A. Ishii, J. P. Bradley, J. Gillis-Davis, J. A. McFadden, M. S. Thompson, R. Christoffersen, L. P. Keller, J. I. Simon, F. M. McCubbin, R. A. Zeigler, J. Gross, R. A. Ketcham, R. D. Hanna, D. Edey, the ANGSA Science Team, Revealing the moon's Taurus-Littrow landslide via integrated analysis of Pristine Apollo 17 Soil Core 73001/2. *J. Geophs. Res. Planets* **130**, e2024JE008556 (2025).
14. M. S. Robinson, B. L. Jolliff, "The landslide that is not," in *44th COSPAR Scientific Assembly* (The SAO Astrophysics Data System, 2022), p. 276.
15. H. H. Schmitt, E. A. Cernan, "A geological investigation of the Taurus-Littrow valley," in *Apollo 17 Preliminary Science Report* (NASA SP-330, 1973); www.nasa.gov/wp-content/uploads/static/history/alsj//a17/as17psr.pdf.
16. S. Le Mouélic, P. Enguehard, H. H. Schmitt, G. Caravaca, B. Seignovert, N. Mangold, J.-P. Combe, F. Civet, Investigating lunar boulders at the Apollo 17 landing site using photogrammetry and virtual reality. *Remote Sens. (Basel)* **12**, 1900 (2020).
17. H. J. Hovland, J. K. Mitchell, Boulder tracks and nature of lunar soil. *Moon* **6**, 164–175 (1973).
18. R. Arvidson, R. J. Drozd, C. M. Hohenbert, C. J. Morgan, G. Poupeau, Horizontal transport of the regolith, modification of features, and erosion rates on the lunar surface. *Moon* **13**, 67–79 (1975a).
19. R. Arvidson, G. Crozaz, R. J. Drozd, C. M. Hohenberg, C. J. Morgan, Cosmic ray exposure ages of features and events at the apollo landing sites. *Moon* **13**, 259 (1975).
20. N. A. Petersson, Serpentine Wave Propagation (Lawrence Livermore National Laboratory, 2010); https://computing.llnl.gov/projects/serpentine-wave-propagation/software.
21. K. Onodera, T. Kawamura, S. Tanaka, Y. Ishihara, T. Maeda, Quantitative evaluation of the lunar seismic scattering and comparison between the Earth, Mars, and the Moon. *J. Geophs. Res. Planets* **127**, e2022JE007558 (2022).
22. D. E. Smith, M. T. Zuber, G. A. Neumann, F. G. Lemoine, E. Mazarico, M. H. Torrence, J. F. McGarry, D. D. Rowlands, J. W. Head III, T. H. Duxbury, O. Aharonson, P. G. Lucey, M. S. Robinson, O. S. Barnouin, J. F. Cavanaugh, X. Sun, P. Liiva, D.-D. Mao, J. C. Smith, A. E. Bartels, Initial observations from the Lunar Orbiter Laser Altimeter (LOLA). *Geophy. Res. Letts.* **37**, L18204 (2010).
23. A. Frankel, R. W. Clayton, Finite difference simulations of seismic scattering: Implications for the propagation of short-period seismic waves in the crust and models of crustal heterogeneity. *J. Geophys. Res.* **91**, 6465–6489 (1986).
24. N. A. Teanby, J. Wookey, Seismic detection of meteorite impacts on Mars. *J. Phy. Earth Planet. Interiors* **186**, 70–80 (2011).
25. J. Oberst, Unusually high stress drops associated with shallow moonquakes. *J. Geophys. Res.* **92**, 1397–1405 (1987).
26. P. Mahanti, M. S. Robinson, T. J. Thompson, M. R. Henriksen, Small lunar craters at the Apollo 16 and 17 landing sites - Morphology and degradation. *Icarus* **299**, 475–501 (2018).
27. T. R. Watters, M. S. Robinson, R. A. Beyer, M. E. Banks, J. F. Bell III, M. E. Pritchard, H. Hiesinger, C. H. van der Bogert, P. C. Thomas, E. P. Turtle, N. R. Williams, Evidence of recent thrust faulting on the Moon revealed by the Lunar Reconnaissance Orbiter Camera. *Science* **329**, 936–939 (2010).
28. T. R. Watters, M. S. Robinson, G. C. Collins, M. E. Banks, K. Daud, N. R. Williams, M. M. Selvans, Global thrust faulting on the Moon and the influence of tidal stresses. *Geology* **43**, 851–854 (2015).
29. S. Stein, M. Wysession, *An Introduction to Seismology, Earthquakes, and Earth Structure*, (Blackwell Publsihing, 2003).
30. T. R. Watters, N. C. Schmerr, R. C. Weber, C. L. Johnson, E. J. Speyerer, M. S. Robinson, M. E. Banks, Tectonics and seismicity of the lunar south polar region. *Planet Sci. J.* **5**, 22 (2024).
31. S. Hassan, U. El Sham, DEM simulations of the seismic response of granular slopes. *Comput. Geotech.* **112**, 230–244 (2019).
32. A. Dahal, D. A. Castro-Cruz, H. Tanyaş, I. Fadel, P. M. Mai, M. van der Meijde, C. van Westen, R. Huser, L. Lombardo, From ground motion simulations to landslide occurrence prediction. *Geomorphology* **441**, 108898 (2023).
33. N. M. Newmark, Effects of earthquakes on dams and embankments. *Géotechnique* **15**, 139–160 (1965).
34. S. F. Gallen, M. K. Clark, J. W. Godt, Coseismic landslides reveal near-surface rock strength in a high-relief, tectonically active setting. *Geology* **43**, 11–14 (2015).
35. N. E. Demidov, A. T. Basilevsky, Height-to-diameter ratios of moon rocks from analysis of *Lunokhod-1* and *-2* and *Apollo 11–17* panoramas and LROC NAC images. *Sol. Syst. Res.* **48**, 324–329 (2014).
36. Y. Li, A. T. Basilevsky, M. Xie, W.-H. Ip, Shape of boulders ejected from small lunar impact craters. *Planet. Space Sci.* **145**, 71–77 (2017).
37. K. Onodera, New views of lunar seismicity brought by analysis of newly discovered moonquakes in Apollo short-period seismic data. *J. Geophys. Res. Planets* **129**, e2023JE008153 (2024).

Acknowledgments: We thank R. Arrowsmith and an anonymous reviewer for valuable comments and suggestions that greatly improved the manuscript. We also thank C. Nypaver for help in the preparation of the figures. We gratefully acknowledge the LRO engineers and technical support personnel. **Funding:** T.R.W. was supported by the LRO Project and an ASU and Intuitive Machines LROC contract. N.C.S. was supported by NASA SSERVI GEODES grant 80NSSC19M0216. **Author contributions:** Conceptualization: T.R.W. and N.C.S. Methodology: T.R.W. and N.C.S. Investigation: T.R.W. and N.C.S. Visualization: T.R.W. and N.C.S. Funding acquisition: T.R.W. and N.C.S. Writing—original draft: T.R.W. Writing—review and editing: T.R.W. and N.C.S. **Competing interests:** The authors declare that they have no competing interests. **Data and materials availability:** All data needed to evaluate the conclusions in the paper are present in the paper. Data are also available on the Smithsonian's figshare site (https://figshare.com/s/f1c9364c232f4664d483). Lunar Reconnaissance Orbiter Camera CDR, EDR, and RDR products are available from the LROC Archive (http://lroc.sese.asu.edu/data/). The LROC images and mosaics can also be viewed using the LROC QuickMap (https://quickmap.lroc.asu.edu/).

Submitted 1 November 2024
Accepted 2 July 2025
Published 30 July 2025
10.1126/sciadv.adu3201

Science Advances

Paleoseismic activity in the moon's Taurus-Littrow valley inferred from boulder falls and landslides

Thomas R. Watters and Nicholas C. Schmerr

Sci. Adv. **11** (31), eadu3201. DOI: 10.1126/sciadv.adu3201

Science Advances (ISSN 2375-2548) is published by the American Association for the Advancement of Science. 1200 New York Avenue NW, Washington, DC 20005. The title *Science Advances* is a registered trademark of AAAS.